frontiers | Frontiers in Earth Science

TYPE Original Research
PUBLISHED 17 November 2022
DOI 10.3389/feart.2022.1037126

OPEN ACCESS

EDITED BY
Qiangtai Huang,
Sun Yat-sen University, China

REVIEWED BY
Gilles Levresse,
Geosciences Center, National Autonomous University of Mexico, Mexico
Dongya Zhu,
SINOPEC Petroleum Exploration and Production Research Institute, China

*CORRESPONDENCE
Adhipa Herlambang,
adhipa.herlambang@kfupm.edu.sa

SPECIALTY SECTION
This article was submitted to Sedimentology, Stratigraphy and Diagenesis, a section of the journal Frontiers in Earth Science

RECEIVED 05 September 2022
ACCEPTED 25 October 2022
PUBLISHED 17 November 2022

CITATION
Herlambang A, Koeshidayatullah AI, Amao AO, Bello AM, Al-Ghamdi F, Malik MH and Al-Ramadan KAH (2022), Structural diagenesis and dolomitization of Cenozoic post-rift carbonates in the Red Sea rift basin: A multiproxy approach.
Front. Earth Sci. 10:1037126.
doi: 10.3389/feart.2022.1037126

Structural diagenesis and dolomitization of Cenozoic post-rift carbonates in the Red Sea rift basin: A multiproxy approach

Adhipa Herlambang[1]*, Ardiansyah I. Koeshidayatullah[2], Abduljamiu O. Amao[1], Abdulwahab M. Bello[1], Faisal Al-Ghamdi[1], Muhammad H. Malik[2] and Khalid A. H. Al-Ramadan[1,2]

[1]Center for Integrated Petroleum Research, College of Petroleum Engineering and Geosciences, King Fahd University of Petroleum and Minerals, Dhahran, Saudi Arabia, [2]Geosciences Department, College of Petroleum Engineering and Geosciences, King Fahd University of Petroleum and Minerals, Dhahran, Saudi Arabia

Middle Miocene post-rift sediments are considered prolific subsurface reservoirs, representing one of the thickest sequences in the Red Sea rift basin. In the Umm Luj Basin of the eastern Red Sea, post-rift sediments are well exposed and represented by a carbonate-dominated system of the Raghama Formation. This formation was intensely fractured, following the rifting trend of the Red Sea. Such fractures and their associated diagenetic products could provide a significant archive of past tectonic fluid evolution. However, little is known about the origin and timing of the different fluid flows and diagenetic processes in the area. This study aims to resolve this issue by integrating fracture and multiproxy geochemical analyses of calcite precipitated in veins, fault breccia, and dolomitized host rock. The $\delta^{18}O$ and $\delta^{13}C$ isotopic compositions of calcite veins show tight clustering, varying between −10.6 and −9.5‰ and between −7.9 and −7.2‰, respectively. Meanwhile, the precipitated calcite along the fault breccia exhibited a closer to host rock isotopic composition ($\delta^{18}O$ = −6.8‰; $\delta^{13}C$ = −4.8‰). The $\delta^{18}O_{VPDB}$ of the dolomitized host rock shows a heavier average value, closer to the expected range of Miocene seawater. X-ray diffraction analysis shows that the veins have a high magnesium calcite content (up to 79.5%). In contrast, all the host rock samples, except samples 1-1BH, have dolomite contents of up to 94.3%, as well as breccia fragments. Thus, we argue that the structural diagenesis history of the study area comprises two distinct fluid members and tectonic events. The first member is the deposition of heavier isotopic composition related to dolomitization at slightly higher temperatures of up to 42.2°C. The second fluid flow member corresponded to a depleted isotopic calcite member with a temperature of 33°C. Compared with the Midyan Peninsula, the study area shares the same regional tectonic events, but the local tectonic and depositional settings could act as the determining factors of the dolomitization mechanism and meteoric alteration in each location. Hence, our results provide a new understanding of paleo-fluid circulation related to the

evolution of tectonic events and highlights the value of integrating fracture and multiproxy geochemical analysis for structural diagenetic studies.

KEYWORDS

diagenesis, isotope, dolomite, carbonate, vein, Red Sea

Introduction

Several previous works have highlighted the importance of studying deformational structures and chemical changes, known as structural diagenesis (e.g., Eichhubl et al., 2004; Laubach and Ward, 2006; Eichhubl et al., 2009; Laubach et al., 2010; Wu et al., 2019), in unraveling how fractures and fluid flow interact along fracture systems. Despite numerous studies, understanding structural diagenesis, that is, the relationship between fluid flow and structural elements, remains challenging. This is partly because the nature of the contribution of the fracture/fault to fluid flow (e.g., hydrocarbon entrapment, migration, and flow) varies widely (Smith, 1980; Knipe et al., 1998; Odling et al., 1999; Aydin, 2000). This is compounded by the fact that the petrophysical properties of fractures can vary significantly. They are mainly affected by the host rock composition, deformation mechanisms, and stress history (Knipe et al., 1998). Although challenging, structural diagenesis is becoming increasingly essential for a broad range of applications, including extracting hydrocarbon resources (Lander et al., 2008; Laubach et al., 2009) and predicting the behavior of injected fluids in the subsurface (Tsang et al., 2000; Tsang, 2005; Dockrill and Shipton, 2010). In particular, the movement of fluids through open fracture systems in the rift basin setting is of significance due to the combination of episodic fluid flow and fracturing events. This allows the reconstruction of tectonic evolution and paleo-fluid flow in an active tectonic basin. Furthermore, fractures can act as archives for episodic fluid sources when mineral constituents carried by an aqueous solution are deposited through precipitation, forming mineral deposits called veins (Bons, 2000). This fluid circulation may alter limestone into dolomite, when limestone comes into contact with magnesium-rich water. This dolomitization results in intergranular pores that are important for the oil and gas reservoir. In addition to creating pores, the considerable dolomitization also helped to preserve them (Koeshidayatullah et al., 2016).

The Miocene carbonate in the Red Sea Basin is an ideal location for studying paleo-fluid circulation along fractures, due to of the exposed carbonate outcrop and the existence of a network of fractures filled with diagenetic calcite crystals (Al-Ramadan, 2017; Hollis et al., 2017; Al-Ramadan et al., 2019). Carbonate rocks are of particular interest, due to the wide variety of diagenetic modifications that can occur as a result of paleo-fluid circulation along fractures (Stacey et al., 2021a; Stacey et al., 2021b; Koeshidayatullah et al., 2022). Additionally, Miocene carbonates are of both economic and environmental importance. Hydrocarbons have been discovered in mid-Miocene rocks in the northern part of the study area and the Midyan Basin of the Red Sea, along with economic mineral deposits of zinc, lead, and other minerals (Hughes and Johnson, 2005). Moreover, seismic and drilling activities by Saudi Aramco in the 1990s demonstrated the existence of hydrocarbon-bearing carbonate reservoirs in the Midyan region (Hughes et al., 1999).

The basin has a complex structural history, due to the Red Sea Oligocene-Miocene extension tectonics and the Pliocene-recent anticlockwise rotation of the Arabian Plate relative to Africa on the Dead Sea Transform Fault. However, limited tectonic evidence has been obtained in this area. Thus, comparing the Miocene carbonates in the study area to other well-studied areas (i.e., the Midyan) is needed to gather more geological information. Here, we applied stable isotope geochemistry to improve our understanding of the structural diagenetic processes in a rift basin setting. Calcite minerals that precipitated in veins and fractures can be used as archives of the oxygen isotopic composition of the diagenetic fluid and the temperature of precipitation of the mineral (Moore and Wade, 2013). Coupled with the analysis of the mineral composition, this study demonstrates the value of multiproxy analysis for structural diagenetic studies in this area for the first time.

The specific objectives of our study were to 1) reconstruct the isotopic values of the host rock to estimate the temperature of dolomitization of the matrix, 2) constrain the estimated temperature of the various calcite phases that infill the fractures, 3) reconstruct the evolution of diagenetic fluid circulation in fractures based on the results of (1) and (2), and 4) compare the recent results with available Cenozoic post-rift carbonate studies within the Arabian Plate.

Geological background

This study utilized a well-exposed carbonate outcrop in the Red Sea rift basin that is affected by the active tectonic region of the Red Sea rifting. The Red Sea rift basin, located on the eastern side of the Arabian Plate, originated as an Oligocene continental rift due to left-lateral wrenching. The Red Sea basins have a similar tectonic history to the Ifal and Midyan basins in their northeastern part and the Gulf of Suez in their northwestern part throughout the Late Oligocene to Middle Miocene (Tubbs et al., 2014).

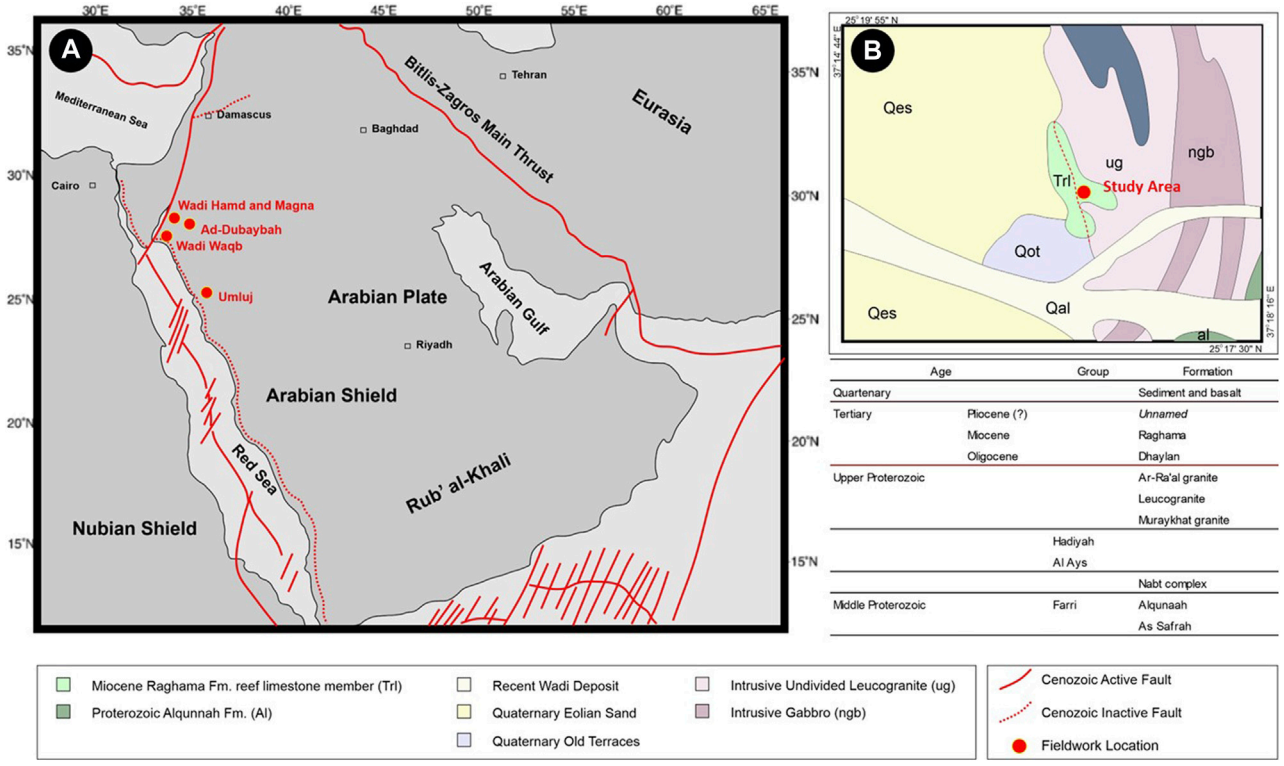

FIGURE 1
Map of the study area. **(A)** Regional tectonic of the Saudi Arabian Plate. The red dots are Umm Luj's recent study area and three previous study areas: Wadi Hamd and Magna, Ad-Dubaybah, and Wadi Waqb (Al-Ramadan, 2017; Al-Ramadan et al., 2019) from the north to the south, respectively. The red box in the Umm Luj indicates the study area. **(B)** Geological map of the Umm Luj study area and table of the lithostratigraphic unit of the study area [modified according to Pellaton (1982)].

The oldest lithostratigraphic unit in the study area is the Precambrian basement, known as the As Safrah and Alqunnah formations, together with various intrusions dating from approximately 800 to 640 Ma (Pellaton, 1982). The basement outcrop is bounded by faults associated with the opening of the Red Sea Rift. Rifting in the Red Sea continues as an episodic process that began in the Permian (Bosworth et al., 2005). Oligocene continental rifting is associated with episodic and segmented movement of the Arabian Peninsula away from Africa (e.g., Bosworth et al., 2005; Tubbs et al., 2014; Almalki et al., 2015). Magmatic expansion resulted in igneous emplacements, and isostatic compensation caused the rift shoulders to undergo uplift and local erosion into rapidly subsiding and tilting block-faulted basins. The base of the syn-rift deposition is dated to 33–34 Ma (Hughes and Johnson, 2005). Likewise, offshore exploration drilling in the northern Red Sea encountered Upper Oligocene nannofossils in the lower syn-rift section (Hughes, 2014). The syn-rift deposition in the study area is represented by the Oligocene Dhaylan Formation, which consists of thin detrital arkose beds and finely bedded red clay. Lenticular layers of reef limestone and well-bedded conglomerate occur locally, overlain by yellow marl containing pebbles (Pellaton, 1982). The Oligocene Dhaylan Formation is unconformably overlain by the Miocene Raghama Formation in some places and is molded on Precambrian basement in others, as a result of tectonic readjustment that took place in the late Early Miocene. This tectonic readjustment facilitated the development of paleo-highs bounded by normal faults and allowed the Raghama carbonate member to exist. Post-rift carbonate and evaporite depositions were extensive until the Pliocene, when open marine conditions were established. The unnamed Pliocene rocks are marked by a paleogeographic split that causes regional unconformities (Pellaton, 1982). Fluviatile terraces, alluvial and eolian deposits, and coral reef limestone just slightly above the present-day sea level constitute the Pleistocene and Quaternary deposits.

Site and samples

Samples were collected from an outcrop at 25°18′00.19″ N 37°16′47.54″ E, 18 km east of the Red Sea coastline, and 35 km from Umm Luj, the nearest city (Figure 1). The study area lies in

the Umm Lajj (or Umm Luj) quadrangle reported by Pellaton (1982). In this report, the outcrop was categorized as a reef limestone member (Trl) of the Miocene Raghama Formation. In the study area, the approximately 20-m-thick Raghama Formation unconformably overlies the granitic basement. Basal reef limestones have steep primary dips because of the molding of reefs on the Precambrian basement (Pellaton, 1982).

In all, 19 samples were collected from the carbonate matrix of the host rock along two different vein sets, breccia cement, and fragments, and the calcite crystals in the coral fragments were selected for carbon and oxygen isotope analyses. X-ray diffraction (XRD) analysis was performed on 15 of the 19 samples to determine their mineral composition, and 12 representative samples were also prepared for thin sections for petrographic analysis and scanning electron microscopy (SEM).

In addition, the 54 carbon and oxygen isotopic data points from Miocene carbonate situated in the Midyan Peninsula at four different locations, Wadi Waqb, Ad-Dubaybah, Wadi Hamd, and Magna, were re-visited in this study (Al-Ramadan, 2017; Al-Ramadan et al., 2019).

Methods

All laboratory analyses were performed in-house at the King Fahd University of Petroleum and Minerals, Saudi Arabia. For this purpose, 12 thin petrographic sections representing the host rock and three different facies (upper, middle, and lower facies) were prepared to characterize the diagenetic products and microfacies of the host rock sample following the Dunham (1962) and Embry and Klovan (1971) classifications (Dunham, 1962; Embry and Klovan, 1971). A Zeiss Axioscan Z1 automated slide scanning system equipped with various lenses and a sophisticated focusing method for high-resolution imaging was employed for petrographic acquisition and analysis. The representative rock chips were mounted on pin-type stubs for analysis by scanning electron microscopy (SEM). To understand the microscale interactions between the hostrock, fractures, and their associated diagenetic products, high-resolution images were acquired using a Zeiss Crossbeam 550 SEM following the method proposed by Amao et al. (2016).

Finely ground powders from 13 samples were used for mineral identification and quantitative phase analysis using powder XRD. XRD analysis was performed using an in-house Empyrean Malvern Panalytical instrument. The results were fitted using the Rietveld method and processed using proprietary Malvern PANalytical HighScore Plus software. The XRD start position for 2θ was 4°, and the ending position was at 70°, with a step size of 0.013°. The scan time step was 8.67, continuously.

Stable carbon and oxygen isotope analyses were performed on the carbonate samples to determine the geochemical conditions and precipitation temperatures. Sampling using micro-drilling techniques was attempted to avoid contamination of calcite veins with carbonate host rock and, when possible, to analyze carbonate cement at various points within the host rock. Thus, 80–100 μg powders were reacted with 102–105% phosphoric acid at 70°C for 480 s for calcite and at 70°C for 720 s for dolomite before CO_2 gas was liberated to the automated purification line. The product CO_2 was then purified using cryogenic traps to eliminate contaminant gases produced during the acid digestion of the carbonate samples, such as water vapor and non-condensable gases. The purification was performed automatically using a Kiel IV carbonate device. The CO_2 gas released was collected and analyzed using a Thermo Finnigan MAT-253 plus mass spectrometer with an overall precision of 0.04‰ for $\delta^{13}C$ and 0.08‰ for $\delta^{18}O$. The oxygen and carbon isotope data are presented in δ notation relative to the Vienna Pee Dee Belemnite (VPDB) standard. The conversion from VPDB (δ_{VPDB}) to SMOW (δ_{SMOW}) follows the equation of Anderson and Arthur (1983): $\delta_{SMOW} = 1.03086\ \delta_{VPDB} + 30.86$.

The measurements on a mass spectrometer drift over time for many reasons, such as ion source performance (D'Autry et al., 2010) or the presence of contaminants. The drift was corrected by plotting the raw $\delta^{18}O$ and $\delta^{13}C$ data against the internal carbonate standards (KIS; KFUPM Iceland Sparite) with the accepted isotopic values of -6.23‰ and 2.25‰ for $\delta^{18}O$ and $\delta^{13}C$ respectively.

The precipitation temperature of calcite samples was estimated based on the following oxygen isotope fractionation between calcite and water by Kim and O'Neil (Kim and O'Neil, 1997): $\delta^{18}O_{cal} - \delta^{18}O_{SW} = ((18.03\ (10^3))/T—273.15)—32.42$, where T is the temperature of the water in which the calcite precipitated (°C), $\delta^{18}O_{cal}$ are the values of $\delta^{18}O$ for the calcite sample (SMOW), and $\delta^{18}O_{SW}$ is the value of $\delta^{18}O$ of the water (SMOW).

For comparison, the estimated temperature of calcite is also defined as follows (Erez and Luz, 1983; Zachos et al., 1994; Stewart et al., 2004): $T = 16.998 - 4.52\ (\delta^{18}O_{cal} - \delta^{18}O_{SW}) + 0.03\ (\delta^{18}O_{cal} - \delta^{18}O_{SW})^2$. We also compared the estimated temperatures based on O'Neil et al. (1969). The equation for estimated temperature is defined as follows: $T = 16.9 - 4.38\ (\delta^{18}O_{cal} - \delta^{18}O_{SW})$, where T is the temperature of the water in which the carbonate precipitated (°C), $\delta^{18}O_{cal}$ are the values of $\delta^{18}O$ for the calcite sample (VPDB), and $\delta^{18}O_{SW}$ is the value of $\delta^{18}O$ of the water (SMOW), respectively.

By contrast, Epstein et al. (1953) developed an equation for calcite paleotemperature that is used to calculate the "isotope temperature" of calcite formation more directly by providing the $\delta^{18}O$ value of the water from which the calcite precipitated. The isotope temperature is defined as follows: $T = 16.5 - 4.3\ (\delta^{18}O_{cal}) + 0.14\ (\delta^{18}O_{cal})^2$, where T is the temperature in °C (based on a least-squares fit for a range of temperature values between 9 and 29°C, with a standard deviation of ±0.6°C), and $\delta^{18}O_{cal}$ is $\delta^{18}O$ for a calcite sample (VPDB).

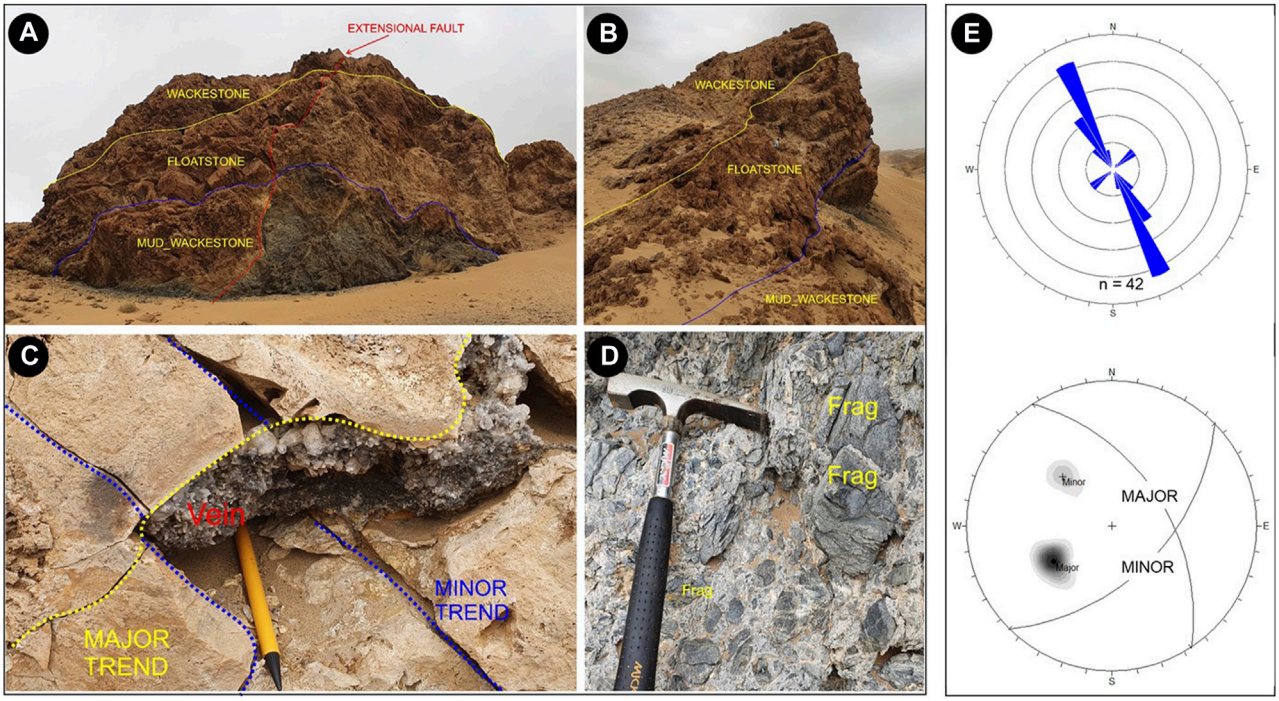

FIGURE 2
Outcrop image of the study area. **(A)** Three different facies are observed: lowermost mud-wackestone, middle coralline floatstone, and uppermost wackestone. The red line points to an extensional fault. **(B)** Outcrop image from a different angle shows 30–40° dipping to the NW. **(C)** Two dominant fracture trends: major (yellow dash line) and minor trend (blue dash line), with partial dog tooth-shape vein filling. **(D)** Breccia zone consists of sidewall carbonate fragments (Frag: Breccia fragment). **(E)** Top picture is a rosette diagram of kinematic vein analysis in the study area. The bottom picture is the bed plane in a contour plot showing the major trend of both major and minor vein's strike and dip direction.

For the dolomite samples, the estimated paleotemperature followed the dolomite-water fractionation equation of Horita (2014): $\delta^{18}O_{dol} - \delta^{18}O_{SW=}((3.14\ (10^3)/T^2\text{-}273.15)—3.14$, where T is the temperature of the water in which the dolomite precipitated (°C), $\delta^{18}O_{dol}$ are the values of $\delta^{18}O$ for the dolomite sample (SMOW), and $\delta^{18}O_{SW}$ is the value of $\delta^{18}O$ of the water (SMOW).

Results

Fracture characteristics

Outcrop observations indicate that the outcrop was fractured, and a normal fault with a brecciation zone occurred. The fault direction (N340°E/55°NW) follows the regional Red Sea rifting trend (Figure 2). The brecciation zone is made up of more than 50% of rock fragments from the sidewall carbonate host rock. The breccia fragments are dominated by mud-wackestone and coralline floatstone limestones. From local structural studies at the outcrop, two distinguished dog tooth-shaped crystal vein sets were observed: N330°E/55°NW (major vein) and N40°E/55°SE (minor vein). The major vein appears more in the outcrop than in the minor vein. Both fracture sets are categorized as extensional fractures with syntaxial calcite filling or veins and are identical in geometry but have slightly perpendicular orientations. Moreover, both fractures were more numerous and intense closer to the fault.

Microfacies

The thin section resulted in the lowermost facies being classified as mud-wackestone, followed by the middle facies characterized as floatstone (Figure 3A) and the upper facies as wackestone, confirming the initial field observation. In the lower part of the outcrop, the boundary between the sediment and basement is marked by a rubble zone, where sizeable boulders of the basement float in very fine, creamy fossiliferous carbonate. A sandy carbonate layer in the middle strata followed this layer, with thin laminated mud layers. An abundance of *Borelis melo* has been observed in this stratum, confirming its Miocene age (Hughes, 2014; Koeshidayatullah et al., 2016). The last unit is marked by a very thick (10.75 m) floatstone coral unit at the bottom, followed by a 3-m wackestone to the top (Figure 2).

The petrographic analysis (Figure 3) of all facies indicates the presence of micritized skeletal grains and isopachous cement.

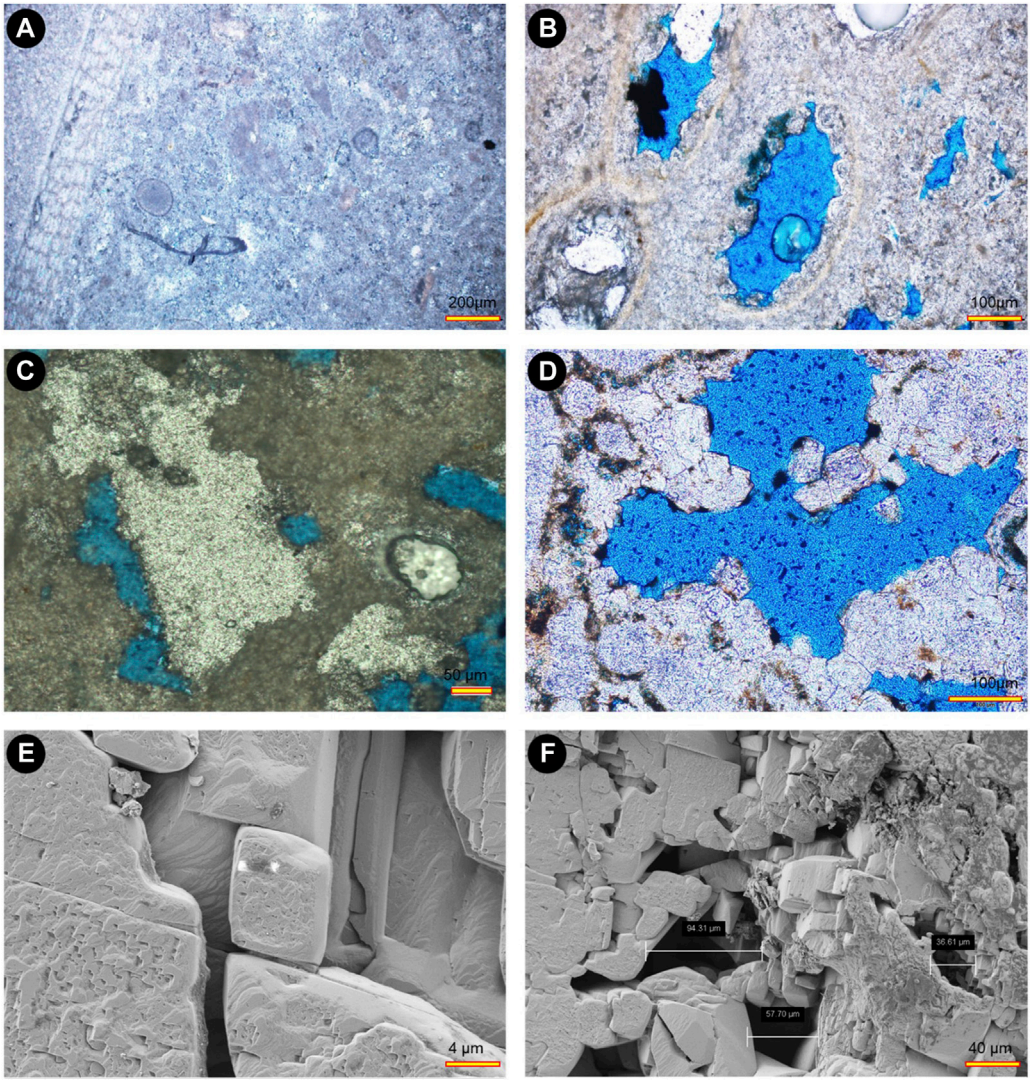

FIGURE 3
Petrographic images of the samples. **(A)** Image shows the thin section of coralline floatstone facies. **(B)** Image shows the fossil grain's partial dissolution, creating a moldic porosity. **(C)** Blocky-drusy calcite cement replacement represents a brighter color. **(D)** Dolomite crystal sizes range from 50 to 100 µm, and the dolomite crystals have euhedral and subhedral textures. **(E)** and **(F)** pictures are the SEM images for the dolomite crystals. **(F)** Image exhibits the micropores between dolomite crystals.

Drusy to block cement replacement also appeared within the samples (Figure 3C). Furthermore, all dolomite is present as a replacement phase for the matrix and grains in varying degrees, fully or partially. Dolomite crystals with sizes ranging from 50 to 100 µm have euhedral and subhedral textures (Figures 3D,E). The porosity types within the sample were abundant inter-intragranular and moldic porosities from partial and complete dissolution (Figure 3B), as well as micropores between dolomite crystals (Figure 3F).

Mineralogy

The XRD results are listed in Table 1. All carbonate veins had a high magnesium calcite content (up to 79.5%). Moreover, all the host rock samples, except samples 1-1BH, had dolomite contents that varies from 23.4 to 94.3%, as well as breccia fragments (98.7% dolomite content). The SEM images (Figure 3) confirmed the XRD results for dolomite content in the host rock samples.

10.3389/feart.2022.1037126

TABLE 1 Summary of isotope and XRD analysis of the study area.

Area and sample ID	Formation	δ13C	Calc [VPDB] [‰]	S.E	δ18O	Calc [VPDB] [‰]	S.E	Calcite [%]	Dolomite [%]	Magnesium calcite [%]	Goethite [%]	Quartz low [%]	Roedderite [%]	Other [%]
Host rock														
1-1AH		−1.29	±	0.00	−2.02	±	0.00	65	35	80.4	2.7			
1-1BH		−3.58	±	0.00	−3.01	±	0.01	16.9	0			5.5	5.5	0.3
3H		−1.32	±	0.01	−2.78	±	0.01		94.5			4.4	4.4	
2-1BH		0.31	±	0.00	−1.09	±	0.00	9.9	60.2	25.5		9.6	9.6	
1-2H		−1.16	±	0.00	−2.12	±	0.00		23.4	67				
Major vein														
1-1B		−7.70	±	0.00	−9.48	±	0.01	54.6		45.4				
1-1A		−7.22	±	0.00	−10.37	±	0.01	34.5		65.5				
1-2W		−7.20	±	0.01	−10.63	±	0.01	20.1		79.5				0.4
1-2B		−8.27	±	0.00	−10.38	±	0.00	47.1		50.3		2.5	2.5	0.1
1-3A		−7.94	±	0.00	−10.61	±	0.01							
1-3B		−7.87	±	0.00	−9.84	±	0.01							
Major vein	Raghama													
2-1A		−7.52	±	0.00	−10.01	±	0.01	31.7		68.3		0.1	0.1	
2-1B		−8.20	±	0.01	−10.12	±	0.01	53.2		41.3				5.5
2-3A		−7.46	±	0.00	−9.47	±	0.01							
Calcite vein in coralline host rock														
2-2		−6.27	±	0.00	−9.34	±	0.01	47.3		49.3		0.2	0.2	3.2
3		−5.87	±	0.00	−7.98	±	0.01	42	0.1	57.8				
3-1		−6.04	±	0.01	−8.09	±	0.01							
Fault breccia			±			±								
BR fragment		−2.82	±	0.00	−2.19	±	0.00		98.7					1.3
BRG cement		−4.83	±	0.02	−6.84	±	0.03	18.2					8.18	

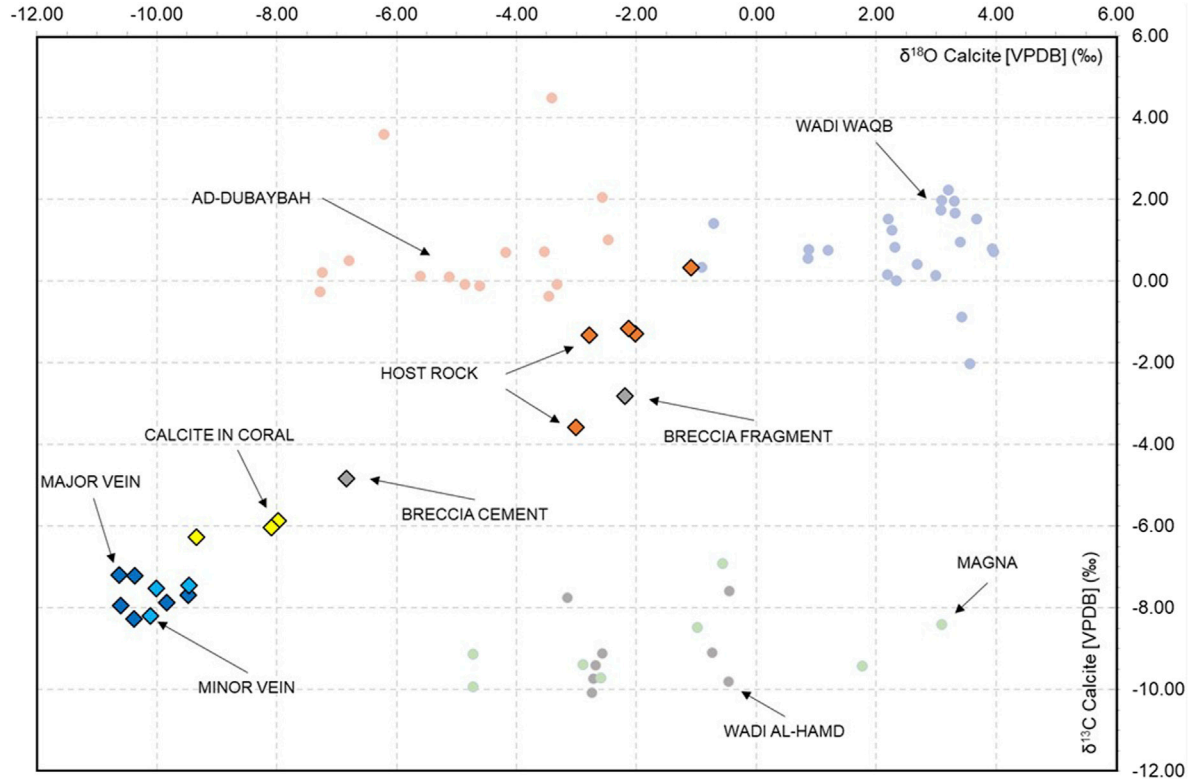

FIGURE 4
Graph plot between $\delta^{13}C_{VPDB}$ and $\delta^{18}O_{VPDB}$ of the study area, with the background data from the previous study of Cenozoic carbonate in the Eastern Red Sea.

Stable isotopes

The isotope analysis results for the samples are presented in Table 1 and Figure 4. The oxygen isotope composition of the host rock samples ($\delta^{18}O_{VPDB}$) ranged from −3.0 to 1.1 ± 0.01‰. The host rock's carbon isotopic ratio ($\delta^{13}C_{VPDB}$) ranged from −3.6 to 0.3‰ ± 0.01‰. The major vein isotopic composition varied from −10.6 to −9.5 ± 0.01‰ and −8.3 to −7.2 ± 0.01‰ for $\delta^{18}O_{VPDB}$ and $\delta^{13}C_{VPDB}$, respectively. Meanwhile, the minor vein isotopic composition varies from −10.1 to 9.5 ± 0.01‰ and −8.2 to 7.5 ± 0.01‰ for $\delta^{18}O_{VPDB}$ and $\delta^{13}C_{VPDB}$, respectively.

The calcite crystals in the coral fragments show the $\delta^{18}O_{VPDB}$ values of −9.3 to 7.9 ± 0.01‰ and $\delta^{13}C_{VPDB}$ values of −6.3 to 5.9‰. Furthermore, the breccia $\delta^{18}O_{VPDB}$ values were −6.8 ± 0.03‰ and −2.2‰ for the cement and fragment, respectively. The breccia cement $\delta^{13}C_{VPDB}$ is −4.8 ± 0.02‰, and the breccia fragment $\delta^{13}C_{VPDB}$ is −2.8‰.

Discussion

In general, the Miocene Raghama Formation situated in the Umm Luj area records a succession of heterogeneous carbonate facies: mud-wackestone, floatstone, and wackestone from the lowermost to the uppermost part, respectively. The carbonate host rocks are mostly dolomitized, as indicated by petrographic and geochemical-coupled analyses. Two dominant fractures were observed, major and minor, with orientations of N330°E/55°NW and N40°E/55°SE, respectively. It is suggested that the veins occurred appeared at a late stage due to uplift.

Origin and depositional setting of the carbonate host rock in the Umm Luj area

Oxygen and carbon isotopes in carbonates are commonly used as paleoclimate proxies. For example, carbonate sediments deposited in typical marine settings have $\delta^{13}C$ values ranging from 0 to 4‰ (Hudson, 1977). Utilizing the carbon and oxygen isotopic composition, the depositional settings of the carbonate host rock can be inferred by the following equation (Narayanan et al., 2007): $Z = 2.048\ (\delta^{13}C_{carb} + 50) + 0.498\ (\delta^{18}O_{carb} + 50)$, where $\delta^{18}O_{carb}$ and $\delta^{13}C_{carb}$ are the $\delta^{18}O$ values and $\delta^{13}C$ values for the carbonate sample (VPDB), respectively. Carbonate host rocks with Z values above 120 are classified as marine, those with values below 120 as freshwater types, and those with Z values

TABLE 2 Calculated paleotemperature of host rock samples.

Area and sample ID	Temperature[a] [°C]	Temperature[b] [°C]	Temperature[c] [°C]	Temperature[d] [°C]	Temperature[e] [°C]
Umluj-Host rock					
1-1AH					38.6
1 1BH	29.0	28.3	30.7	24.5	
3H					42.4
2-1BH					31
1-2H					39.1

[a]Duncan et al., 2004; James et al., 1994; Erez and Luz, 1983.
[b]O'Neil et al., 1969.
[c]Epstein and Lowenstam, 1953.
[d]Kim and O'Neil, 1997.
[e]Horita, 2014.

near 120 as intermediate. All the carbonate host rocks (Z = 123.2–127.4) indicate a marine depositional environment, except for sample 1-1BH (Z=118.5), which was classified as intermediate.

The diagenetic features of the petrographic analysis also support a shallow marine depositional environment. The features associated with this environment were microbial micritization and dolomitization (Figure 3). The creation of micrite envelopes by microboring organisms surrounding skeletal and non-skeletal grains may provide a substrate for a developing marine cement (Al-Ramadan et al., 2019). The depositional environment of the carbonate host rock is suggested to have been deposited in the platform interior to platform margin carbonate facies, characterized by a highly heterogeneous vertical succession (Koeshidayatullah et al., 2016; Al-Ramadan, 2017; Al-Ramadan et al., 2019). The dolomitization process is interpreted to be near-surface, early formed dolomite, based on its fabric-preserving mimetic texture (e.g., Sibley and Gregg, 1987; Swart, 2015).

A summary of the estimated paleotemperature (Table 2) was derived from the calculated $\delta^{18}O$ value of the calcite host rock sample. The paleotemperature calculation is based on the Miocene composition of seawater ($\delta^{18}O_{SW}$), estimated to be −0.4‰ (Lear et al., 1979; Stewart et al., 2004). The difference between the calculated paleotemperatures from the four equations for calcite precipitation in the host rock (sample code is 1-1 BH), was ±5 °C. In detail, the estimated temperatures were 29°C, 28.3°C, 30.7°C, and 24.5°C following the equation of Erez and Luz (1983), Zachos et al. (1994), Stewart et al. (2004), O'Neil et al. (1969), Epstein and Lowenstam (1953), and Kim and O'Neil (1997), respectively. Meanwhile, the dolomite host rocks indicated higher temperatures of up to 42°C, following the equation of Horita (2014). The calculated paleotemperature of the calcite host rock was in close agreement with the Neogene seawater temperature of estimated 30°C (Vérard and Veizer, 2019). This likely indicates that the calcite host rock is represented by pristine seawater. However, the calculated paleotemperature for dolomitic host rocks showed a higher temperature range of 34–42°C. These estimated temperatures match the Miocene carbonate in the Ad-Dubaybah area of Saudi Arabia, with a clumped isotope-derived temperature of 45°C (Al-Ramadan et al., 2019). The elevated temperature is unlikely to be due to the burial realm because the samples are absent from intensive compaction in the form of grain interpenetration, stylolitization, or typical high-temperature dolomite textures, such as anhedral to saddle dolomite in thin sections.

The depleted $\delta^{18}O_{dol}$, light $\delta^{18}O_{SW}$, and slightly elevated temperatures suggest that the fluids might have originated from modified and slightly elevated temperature seawater (Davies and Smith, 2006; Hendry et al., 2015; Martín-Martín et al., 2015). Moreover, the estimated temperature for dolomitic host rocks shows only slightly higher temperature ranges from 34 to 42°C, which may also exhibit a near-surface dolomitization mechanism. The absence of high-temperature dolomitization may be attributed to relatively simple tectonics (Hollis et al., 2017). The dolomitization model that seems suitable for explaining the slightly elevated temperature without the burial process is fault-controlled dolomitization, which involves seawater modification (Figure 5). The dolomitic mechanism related to fault-controlled dolomitization involves seawater modification, which explains the relatively lower temperature of the calcite host rock (1-1BH) occurring at the same outcrop. The fault affects the limited distribution of dolomitized host rock, as the dominant calcite sample of 1-1BH was taken from a relatively distal spot from the fault zone. The limited distribution of dolomite within the study area is associated with a fault that can be used as a pathway (Bons et al., 2012) for modified warmer seawater to ascend and dolomitize adjacent carbonate rocks.

The fact that dolomitization occurred through the circulated seawater is also supported by the highest dolomite content (94.3%) in the coral-dominated host rock. Thus, the coral preserved the primary pores, which are the two primary transport mechanisms for fluids circulating in the rock fabric,

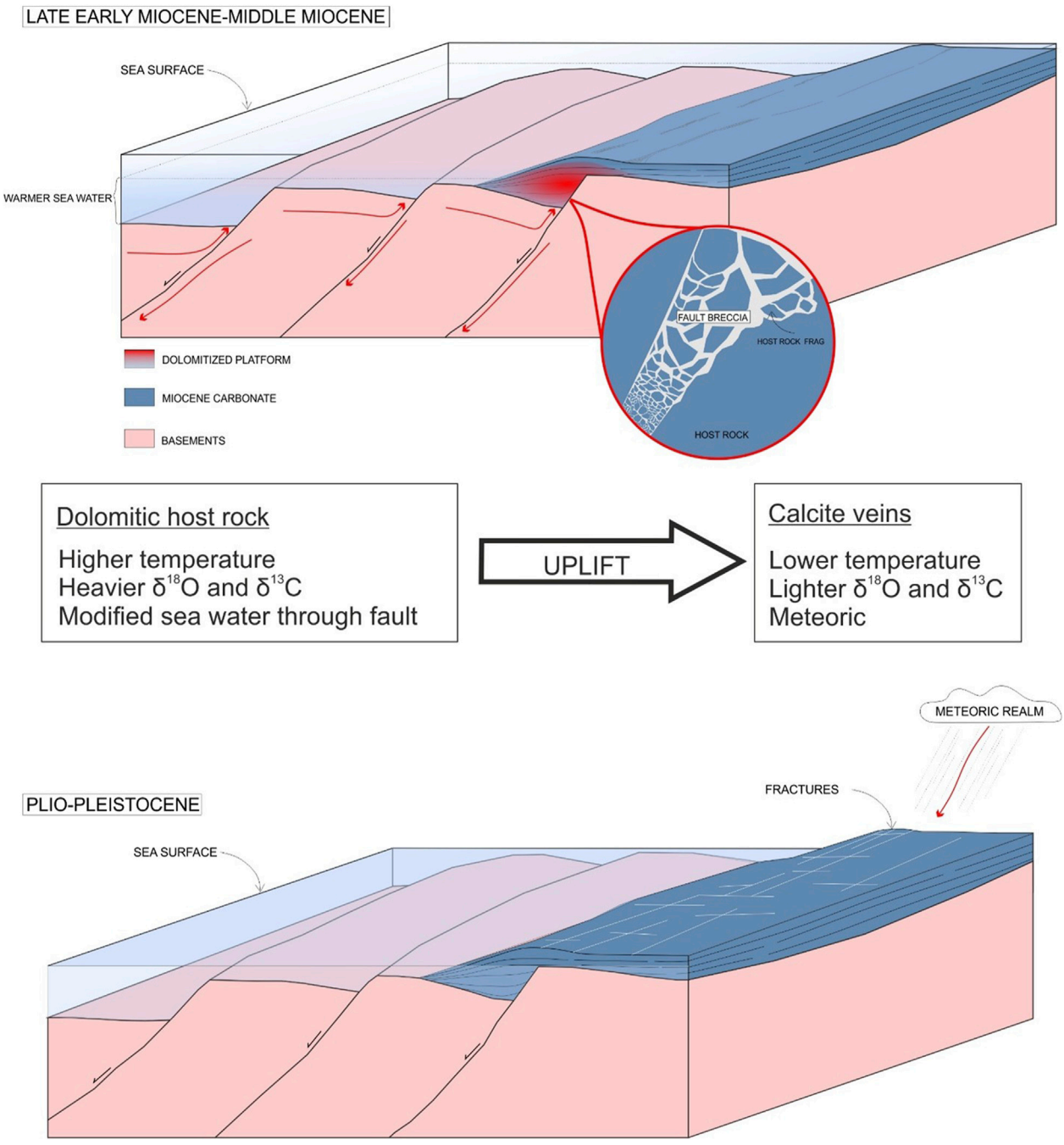

FIGURE 5
Dolomitized model schematic diagram of the Umm Luj study area during the Miocene, then uplift in the Plio-Pleistocene. The later calcite veins indicated the meteoric isotopic signal was encountered from the study area.

that is, pores and fractures (Bons et al., 2012). The main requirements are an effective pumping mechanism and sediments with suitable permeabilities to allow focused flushing of large fluid volumes and to create dolomite (Warren, 2000).

In addition, the low quartz content within the host rock may indicate land attach depositional settings with an active continental input during the Miocene, where the nature of the basin architecture allows an active meteoric fairway to develop and interact with the carbonate platform.

Fluid origin of the calcite vein and fault breccia

Carbonate precipitated in veins and fractures can be used as an archive for the oxygen isotopic composition of the diagenetic fluid and the temperature of precipitation of the mineral (Moore and Wade, 2013). Previous integrated studies combining paleo-thermometry analysis, such as stable isotope and fluid inclusion analysis (e.g., Kenis et al., 2000; Immenhauser et al., 2007; Reuning et al., 2009; Vandeginste and John, 2012; Vandeginste et al., 2017; Koeshidayatullah et al., 2020), have been conducted to reconstruct fluid origin and temperature from fracture-related samples. The $\delta^{18}O$ values of calcite decrease with increasing temperature (Moore and Wade, 2013; Hoefs, 2019). Moreover, oxygen isotopes reflect the temperature dependence of the isotopic fractionation between carbonate and the water in which it grows (e.g., McCrea, 1950; Epstein et al., 1953; O'Neil et al., 1969; Kim and O'Neil, 1997; Horita, 2014). The oxygen isotopes, however, do not provide a direct paleo-thermometer, and temperature reconstructions rely on independent estimates of water isotopic compositions. This is because ^{18}O in carbonates is a function of both the origin fluid composition and the temperature of the mineral precipitates. Thus, it is necessary to know the other parameter to estimate either of the two.

The variation in isotopic oxygen values can represent precipitation from different fluids at different temperatures during the separate cementation phases. Hence, subsurface fluids have various values, ranging from $\delta^{18}O_{VPDB} = -20 \pm 12‰$ VPDB (Land and Prezbindowski, 1981), which have low $\delta^{18}O_{VPDB}$ values and range between −20 and 5‰ VPDB (Hudson, 1977). The vein samples in this study showed a narrow range of $\delta^{18}O_{VPDB}$ values from −10.6 to 9.5 ± 0.01‰. Using the estimated value of the typical rain-water oxygen values for the Arabian Plate during the Neogene and Quaternary, which are difficult to constrain due to paleogeographic variations but are suggested from the groundwater data gathered in Oman, less depleted values of $\delta^{18}O_{VPDB}$ of −13 to −6‰ are found (Fleitmann et al., 2003). The annual ground temperature at the water table is 33 ± 0.3°C (Weyhenmeyer et al., 1979), the origin of the fluid ($\delta^{18}O_{SW}$) of the veins are −5.3 to −6.7‰. However, a more advanced geothermometer technique is required to obtain more precise paleotemperature values. The $\delta^{18}O_{VPDB}$ and $\delta^{13}C_{VPDB}$ values from the vein samples were almost identical to the values of the meteoric cement of a previously taken sample in the Magna area, Saudi Arabia (Al-Ramadan, 2017); see Figure 4. Meteoric water typically has very light oxygen isotope compositions due to evaporative fractionation of the oxygen isotopes, and as a result, calcite precipitated from the meteoric water also has very light oxygen isotope compositions (Hays, Grossman, 1991; Zhu et al., 2019). Therefore, the samples in this study that have comparable isotopic oxygen values within this range could be influenced by meteoric fluids. According to this meteoric origin, high magnesium calcite content in veins from XRD analysis is usually observed in many natural low-temperature environments (e.g., Stanienda-Pilecki, 2018). The veins in this study are likely to precipitate on the relatively more meteoric realm at a later stage because their isotopic signature and dog tooth-shaped crystals may also indicate that meteoric waters influenced the precipitating fluids.

The fragment from brecciated fault zone samples indicated closer isotopic composition to the host rock of −2.2 ± 0.00‰ and −2.8 ± 0.00‰ for $\delta^{18}O_{VPDB}$ and $\delta^{13}C_{VPDB}$, respectively. This similar isotopic value and dolomite content between the breccia fragment and host rock indicate that the breccia fragment is derived from the sidewall host rock. Brecciated wall rocks occur in several fault zones (Woodcock et al., 2006). The breccia consists of more than 30% of the rock mass of visible fragments, classified as fault breccia (Sibson, 1977), and it shows component rotation within the matrix and initial angular to sub-rounded component edges. The rocks into which the solution penetrated at high pressure burst apart and formed angular breccia with components that often do not touch each other (Phillips, 1972). In addition, the roedderite content from the XRD analysis of the breccia cement may indicate a hydrothermal fluid origin that makes contact with a metamorphosed basement and penetrates the fault zone.

Structural diagenesis and paragenetic sequence evolution of Miocene syn-rift carbonates, Umm Luj area

The common interaction phenomenon between the fluid and host rock is host-rock buffered and affects the isotopic signature of the vein (e.g., Sharp et al., 2005; Wagner et al., 2010), especially in calcite veins (e.g., Suchy et al., 2000; Quandt et al., 2019; Chenrai et al., 2022). Therefore, vein signatures should be compared to the stable isotopic signatures of the host rock. When the fluid is buffered, the vein signature is similar to the stable isotopic signature of the host rock, as the precipitating fluids interact with the host rock and adopt its signature. In carbonates, the carbon isotopic signature is much more likely to be host-rock buffered than oxygen isotopic signature (Vrolijk and Sheppard, 1991). This occurs because circulating fluids generally contain sufficient oxygen; thus, oxygen is rarely transferred from the host rock into the fluid. However, most fluids in carbonate systems are poor in carbon content. Therefore, fluid–rock interactions often transfer carbon from the host rock into fluids.

The results of this study prompt the interpretation that the vein isotopic composition preferentially exhibits a non-host rock buffered condition. Because all vein sample isotopic compositions are depleted in carbon and oxygen relative to marine sediments, calcite, precipitated in an open meteoric system (with a low rock/water ratio), is depleted in carbon and oxygen. Hence, it can be

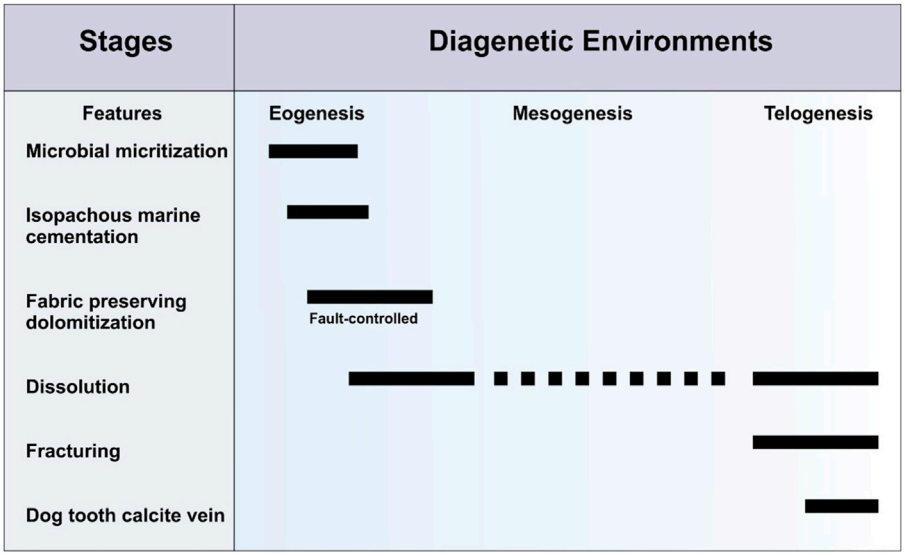

FIGURE 6
Paragenetic sequence of the study area.

concluded that the calcite vein is precipitated in an open system, with a decent volume of fluids involved, and most likely, without any evidence of significant host rock buffered. The timing for the vein is suggested to be present in a relatively late stage because of its isotopic signature, lower temperature regime, and the dogtooth-shaped crystals, indicating that the meteoric waters influenced the precipitating fluids.

On the other hand, the breccia cement indicates a slightly more host-rock buffered condition than vein calcite. The ratio between fragment to matrix appears from the outcrop, and the high roedderite content from the XRD indicates that the brecciation process is related to the hydrothermal process. Hydrothermal activities are postulated to be due to the continuous opening of the Red Sea rift (Vita-Finzi, 2001). This type of hydrothermal-related vein is commonly enriched with ore deposits (Zierenberg and Shanks, 1983). Therefore, this type of fault breccia is suitable for mineral exploration. The timing of this brecciation is interpreted as immediately following the dolomitization of the host rock, indicating that the dolomitic host rock dominated the breccia fragments. In addition, we conclude that the breccia and veins are derived from different fluid sources.

Meanwhile, dolomitization of the host rock occurred in a slightly elevated temperature regime. The suggested mechanism for this dolomitization is fault-controlled dolomitization, which involves seawater modification. The fault is interpreted to be the same fault pathway as the fault breccia, which indicates that the dolomitization and fault movement that led to brecciation occurred at relatively similar events in the Miocene.

Then, the carbonate was exposed and in contact with a more meteoric condition, with both partial and complete dissolution. Partial dissolution is mainly associated with both skeletal and non-skeletal grains (e.g., corals). Moreover, the presence of drusy to blocky replacement cement may also indicate a later stage of meteoric influence on the samples. Finally, calcite precipitated along the younger perpendicular open fracture set. Post-burial meteoric diagenesis is interpreted to be associated with basin-scale uplift during the Plio-Pleistocene opening (Figure 5), with the possibility of existing normal fault reactivation during this time.

Paragenetic sequence evolution of Miocene syn-rift carbonates in the Eastern Red Sea

The Cenozoic carbonate in the eastern Red Sea is suggested to have been dolomitized on a broader tectonic plate scale. The proposed timing of dolomitization of the Cenozoic post-rift carbonates in the eastern part of the Red Sea occurred just after the deposition of the carbonate platforms, while rifting still occurred in the basin (probably in the late Early-Middle Miocene, Figure 6). Although the timing of dolomitization from these five different localities suggests an almost synchronous process, the dolomitization model for each locality is unique. The current study area suggests a dolomitization model related to fault-controlled, modified seawater dolomitization in the early deposition stage, similar to the Ad-Dubaybah area. Meanwhile, dolomitization in the Wadi Waqb area preferentially follows the seepage-reflux dolomitization model (Al-Ramadan et al., 2019). In contrast, Magna and Wadi Alhamd show that dolomitization is due to the uplift and influx of meteoric water in the late stage.

Additionally, this study also confirms that there was an active meteoric influx in post-rift Cenozoic carbonates in the eastern part of the Red Sea before and after the burial process as a ramp attached to the land or an isolated platform setting. Early meteoric diagenesis is observed chiefly in the interior platform part of the Ad-Dubaybah location, even though only very minor evidence of meteoric diagenesis has been observed at the Wadi Waqb locality, suggesting there was active meteoric input during platform emergence at Ad-Dubaybah during Miocene times (Al-Ramadan et al., 2019). Meteoric diagenesis in both areas was revealed by the occurrence of a dogtooth, blocky to drusy cement, and pendent vadose cement. These may represent early meteoric diagenesis. The presence of dedolomitization and non-luminescent calcite fracture filling suggests later meteoric diagenesis. In Magna and Wadi Alhamd, meteoric diagenesis has been interpreted as a product of early diagenesis (eodiagenesis) associated with several episodes of relative sea-level low stands during deposition in the Early Miocene. Subsequently, the peripheral uplift and influx of meteoric water resulted in dolomitization of pre-existing Miocene carbonate (Al-Ramadan, 2017). The meteoric diagenesis in Magna and Wadi Alhamd is characterized by clear blocky and drusy mosaic cement, followed by selective dissolution through the fractures. In this study, meteoric alteration was suggested to have occurred during late diagenesis. Although the low quartz content within the host rock is associated with the interplay between active freshwater input from the hinterland that brought siliciclastic sediments in the early stage, there is no evidence of meteoric diagenesis. In the late stages after uplift, the dog-tooth shape calcite vein originated from a meteoric fluid, suggesting that the study area is in more contact with the meteoric realm. Meteoric diagenesis is indicated by the presence of both partial and complete dissolution of the host rock. Interestingly, compared with Ad-Dubaybah and Wadi Waqb, host rock dedolomitization was not observed in the study area. This fact is suggested to be due to the low degree of fluid–rock interaction.

On a regional scale, the Cenozoic carbonate in the Eastern Red Sea is suggested to have been dolomitized and altered by meteoric influx, but each location has a different mechanism. Hence, the local tectonic and depositional settings might be the determining factors of the dolomitization and alteration mechanisms. The implication of an additional structural diagenetic dataset from the fractures delivers more information for the tectonic evolution of the depositional environment to the diagenetic product within the carbonate, as the Cenozoic carbonate is situated in a fault-bounded platform.

Conclusion

From the dataset, we conclude that 1) the Miocene Raghama Formation situated in the Umm Luj area, which is the eastern part of the Red Sea rifting, records a succession of heterogeneous carbonate facies: mud-wackestone, floatstone, and wackestone from the lowermost to the uppermost part, respectively. The facies represent a variety of settings from the platform interior to the margin. 2) The carbonate host rocks are mostly dolomitized, as indicated by petrographic and geochemical-coupled analyses. The dolomitization mechanism is suggested to have formed early from the modified warmer seawater that ascended along the fault and dolomitized the adjacent carbonate rock. This was evidenced by the estimated paleo-temperature of up to 42.2°C. 3) The carbonate outcrop is intensively fractured, with two dominant fracture types observed: major and minor veins with orientations of N330°E/55°NW and N40°E/55°SE, respectively. 4) The veins are suggested to occur at a late stage owing to uplift. The calcite precipitated along the vein has a light isotopic composition from −10.6 ± 0.01 to −9.5 ± 0.01‰, and is proposed to originate from meteoric water. 5) The study area shares the same regional tectonic events at the basinal scale as the Midyan Peninsula. However, the local tectonic and depositional settings might have determined the dolomitization mechanism and meteoric alteration at each location.

Data availability statement

The original contributions presented in the study are included in the article/Supplementary Material; further inquiries can be directed to the corresponding author.

Author contributions

AH, AK, and KA-R contributed to the conception and design of the study. All authors contributed to the field data collection. FA-G and MM contributed to sample preparation. AH, AK, AA, and AB performed the laboratory analysis and interpretation. AH and AK wrote the first draft of the manuscript. All authors contributed to manuscript revision, and read and approved the submitted version.

Acknowledgments

The authors would like to thank the Geosciences Department, College of Petroleum Engineering and Geosciences, King Fahd University of Petroleum and Minerals. They specially thank Bandar Dhaifallah Al-Otaibi, Habeeb Ahmed Al-Abbas, and all the members of the CIPR (Center for Integrative Petroleum Research) for the help in the laboratory and constructive discussions that resulted in improving the quality of this paper.

Conflict of interest

The authors declare that the research was conducted in the absence of any commercial or financial relationships that could be construed as a potential conflict of interest.

Publisher's note

References

Al-Ramadan, K. (2017). Geochemical signatures of pervasive meteoric diagenesis of early Miocene syn-rift carbonate platform, red sea, NW Saudi Arabia. *Geol. Q.* 61, 239–250. doi:10.7306/gq.1334

Al-Ramadan, K., Koeshidayatullah, A., Cantrell, D., and Swart, P. K. (2019). Impact of basin architecture on diagenesis and dolomitization in a fault-bounded carbonate platform: Outcrop analogue of a pre-salt carbonate reservoir, red sea rift, nw Saudi Arabia. *Pet. Geosci.* 26, 448–461. doi:10.1144/petgeo2018-125

Almalki, K. A., Betts, P. G., and Ailleres, L. (2015). The red sea - 50years of geological and geophysical research. *Earth. Sci. Rev.* 147, 109–140. doi:10.1016/j.earscirev.2015.05.002

Amao, A. O., Al-Ramadan, K., and Koeshidayatullah, A. (2016). Automated mineralogical methodology to study carbonate grain microstructure: an example from oncoids. *Environ. Earth Sci.* 75 (8), 1–11.

Aydin, A. (2000). Fractures, faults, and hydrocarbon entrapment, migration and flow. *Mar. Pet. Geol.* 17, 797–814. doi:10.1016/S0264-8172(00)00020-9

Bons, P. D., Elburg, M. A., and Gomez-Rivas, E. (2012). A review of the formation of tectonic veins and their microstructures. *J. Struct. Geol.* 43, 33–62. doi:10.1016/j.jsg.2012.07.005

Bons, P. D. (2000). The formation of veins and their microstructures. *J. Virt. Ex.* 2. doi:10.3809/jvirtex.2000.00007

Bosworth, W., Huchon, P., and McClay, K. (2005). The red sea and Gulf of aden basins. *J. Afr. Earth Sci.* 43, 334–378. doi:10.1016/j.jafrearsci.2005.07.020

Chenrai, P., Assawincharoenkij, T., Warren, J., Sa-nguankaew, S., Meepring, S., Laitrakull, K., et al. (2022). The occurrence of bedding-parallel fibrous calcite veins in permian siliciclastic and carbonate rocks in Central Thailand. *Front. Earth Sci. (Lausanne).* 9, 1–14. doi:10.3389/feart.2021.781782

D'Autry, W., Wolfs, K., Yarramraju, S., Schepdael, A. Van, Hoogmartens, J., and Adams, E. (2010). Characterization and improvement of signal drift associated with electron ionization quadrupole mass spectrometry. *Anal. Chem.* 82, 6480–6486. doi:10.1021/ac100780s

Davies, G. R., and Smith, L. B. (2006). Structurally controlled hydrothermal dolomite reservoir facies: An overview. *Am. Assoc. Pet. Geol. Bull.* 90, 1641–1690. doi:10.1306/05220605164

Dockrill, B., and Shipton, Z. K. (2010). Structural Controls on Leakage from a Natural CO2 Geologic Storage Site: Central Utah, U.S.A. *J. Struct. Geol.* 32, 1768–1782. doi:10.1016/j.jsg.2010.01.007

Dunham, R. J. (1962). Classification of Carbonate Rocks According to Depositional Texture (1962) Classification of Carbonates Rocks. *Memorian Am. Assoc. Petroleum Geol.* 1, 108–121.

Eichhubl, P., Davatzes, N. C., and Becker, S. P. (2009). Structural and Diagenetic Control of Fluid Migration and Cementation along the Moab Fault, Utah. *Am. Assoc. Pet. Geol. Bull.* 93, 653–681. doi:10.1306/02180908080

Eichhubl, P., Taylor, W. L., Pollard, D. D., and Aydin, A. (2004). Paleo-Fluid Flow and Deformation in the Aztec Sandstone at the Valley of Fire, Nevada - Evidence for the Coupling of Hydrogeologic, Diagenetic, and Tectonic Processes. *Geol. Soc. Am. Bull.* 116, 1120–1136. doi:10.1130/B25446.1

Embry, A. F., and Klovan, E. J. (1971). The Upper Devonian Stratigraphy of Northeastern Banlts Island Has. *Bull. Can. Petroleum Geol.* 19, 730–781.

Epstein, S., Buchsbaum, R., Lowenstam, H. A., and Urey, H. C. (1953). Revised carbonate-water isotopic temperature scale. *Geol. Soc. Am. Bull.* 64, 1315–1326. doi:10.1130/0016-7606(1953)64[1315:rcits]2.0.co;2

Epstein, S., and Lowenstam, H. A. (1953). Temperature-Shell-Growth Relations of Recent and Interglacial Pleistocene Shoal-Water Biota from Bermuda. *J. Geol.* 61, 424–438. doi:10.1086/626110

Erez, J., and Luz, B. (1983). Experimental Paleotemperature Equation for Planktonic Foraminifera. *Geochim. Cosmochim. Acta* 47, 1025–1031. doi:10.1016/0016-7037(83)90232-6

Fleitmann, D., Burns, S. J., Neff, U., Mangini, A., and Matter, A. (2003). Changing Moisture Sources over the Last 330, 000 Years in Northern Oman from Fluid-Inclusion Evidence in Speleothems. *Quat. Res.* 60, 223–232. doi:10.1016/S0033-5894(03)00086-3

Hays, P. D., and Grossman, E. L.1991 Oxygen Isotopes in Meteoric Calcite Cements as Indicators of Continental Paleoclimate. *Geology* 19 (5).

Hendry, J. P., Gregg, J. M., Shelton, K. L., Somerville, I. D., and Crowley, S. F. (2015). Origin, Characteristics and Distribution of Fault-Related and Fracture-Related Dolomitization: Insights from Mississippian Carbonates, Isle of Man. *Sedimentology* 62, 717–752. doi:10.1111/sed.12160

Hoefs, J. (2019). 9th ed., 43. Midtown Manhattan, NY .USA: Springer International Publishing. 9781501508745.Stable Isotope Geochemistry

Hollis, C., Bastesen, E., Boyce, A., Corlett, H., Gawthorpe, R., Hirani, J., et al. (2017). Fault-Controlled Dolomitization in a Rift Basin. *Geology* 45, 219–222. doi:10.1130/G38s394.1

Horita, J. (2014). Oxygen and Carbon Isotope Fractionation in the System Dolomite-Water-CO2 to Elevated Temperatures. *Geochim. Cosmochim. Acta* 129, 111–124. doi:10.1016/j.gca.2013.12.027

Hudson, J. D. (1977)). Stable Isotopes and Limestone Lithification. *J. Geol. Soc. Lond.* 133, 637–660. doi:10.1144/gsjgs.133.6.0637

Hughes, G. W. G., and Johnson, R. S. (2005). Lithostratigraphy of the Red Sea Region. *GeoArabia* 10, 49–126. doi:10.2113/geoarabia100349

Hughes, G. W. (2014). Micropalaeontology and Palaeoenvironments of the Miocene Wadi Waqb Carbonate of the Northern Saudi Arabian Red Sea. *GeoArabia* 19, 59–108. doi:10.2113/geoarabia190459

Hughes, G. W., Perincek, D., Grainger, D. J., Abu-Bshait, A. J., and Jarad, A. R. M. (1999). Lithostratigraphy and Depositional History of Part of the Midyan Region, Northwestern Saudi Arabia. *GeoArabia* 4, 503–542. doi:10.2113/geoarabia0404503

Immenhauser, A., Dublyansky, Y. V., Verwer, K., Fleitman, D., and Pashenko, S. E. (2007). Textural, Elemental, and Isotopic Characteristics of Pleistocene Phreatic Cave Deposits (Jabal Madar, Oman). *J. Sediment. Res.* 77, 68–88. doi:10.2110/jsr.2007.012

Kenis, I., Muchez, P., Sintubin, M., Mansy, J. L., and Lacquement, F. (2000). The Use of a Combined Structural, Stable Isotope and Fluid Inclusion Study to Constrain the Kinematic History at the Northern Variscan Front Zone (Bettrechies, Northern France). *J. Struct. Geol.* 22, 589–602. doi:10.1016/S0191-8141(99)00187-X

Kim, S. T., and O'Neil, J. R. (1997). Equilibrium and Nonequilibrium Oxygen Isotope Effects in Synthetic Carbonates. *Geochim. Cosmochim. Acta* 61, 3461–3475. doi:10.1016/S0016-7037(97)00169-5

Knipe, R. J., Jones, G., and Fisher, Q. J. (1998). Faulting, Fault Sealing and Fluid Flow in Hydrocarbon Reservoirs: An Introduction. *Geol. Soc. Spec. Publ.* 147. doi:10.1144/GSL.SP.1998.147.01.01

Koeshidayatullah, A., Al-Ramadan, K., and Hughes, G. W. (2016). Facies mosaic and diagenetic patterns of the early Devonian (Late Pragian-Early Emsian) microbialite-dominated carbonate sequences, Qasr Member, Jauf Formation, Saudi Arabia. *Geol. J.* 51 (5), 704–721. doi:10.1016/j.marpetgeo.2015.10.017

Koeshidayatullah, A., Al-Sinawi, N., Swart, P. K., Boyce, A., Redfern, J., Hollis, C., et al. (2022). Coevolution of diagenetic fronts and fluid-fracture pathways. *Sci. Rep.* 12 (1), 1–11.

Koeshidayatullah, A., Corlett, H., Stacey, J., Swart, P. K., Boyce, A., Robertson, H., et al. (2020). Evaluating new fault-controlled hydrothermal dolomitization models: Insights from the Cambrian Dolomite, Western Canadian Sedimentary Basin. *Sedimentology* 67 (6), 2945–2973.

Land, L. S., and Prezbindowski, D. R. (1981). The origin and evolution of saline formation water, lower cretaceous carbonates, south-central texas, U.S.A. *Annu. Rev. Earth Planet Sci.* 25, 435–489.

Lander, R. H., Larese, R. E., and Bonnell, L. M. (2008). Toward More Accurate Quartz Cement Models: The Importance of Euhedral versus Noneuhedral Growth Rates. *Am. Assoc. Pet. Geol. Bull.* 92, 1537–1563. doi:10.1306/07160808037

Laubach, S. E., Eichhubl, P., Hilgers, C., and Lander, R. H. (2010). Structural Diagenesis. *J. Struct. Geol.* 32, 1866–1872. doi:10.1016/j.jsg.2010.10.001

Laubach, S. E., Olson, J. E., and Eichhubl, P. (2009). *Unconventional Energy Resources: Making the Unconventional Conventional*.Society for Sedimentary Geology,Tulsa, Oklahoma doi:10.5724/gcs.09.29

Laubach, S. E., and Ward, M. E. (2006). Diagenesis in Porosity Evolution of Opening-Mode Fractures, Middle Triassic to Lower Jurassic La Boca Formation, NE Mexico. *Tectonophysics* 419, 75–97. doi:10.1016/j.tecto.2006.03.020

Lear, C. H., Elderfield, H., and Wilson, P. A. (1979). Cenozoic Deep-Sea Temperatures and Global Ice Volumes from Mg/Ca in Benthic Foraminiferal Calcite. *Science* 287, 269–272. doi:10.1126/science.287.5451.269

Martín-Martín, J. D., Travé, A., Gomez-Rivas, E., Salas, R., Sizun, J. P., Vergés, J., et al. (2015). Fault-Controlled and Stratabound Dolostones in the Late Aptian-Earliest Albian Benassal Formation (Maestrat Basin, E Spain): Petrology and Geochemistry Constrains. *Mar. Pet. Geol.* 65, 83–102. doi:10.1016/j.marpetgeo.2015.03.019

McCrea, J. M. (1950). On the Isotopic Chemistry of Carbonates and a Paleotemperature Scale. *J. Chem. Phys.* 18, 849–857. doi:10.1063/1.1747785

Moore, C. H., and Wade, W. J. (2013). Carbonate Diagenesis: Introduction and Tools. *Dev. Sedimentology* 67, 67–89. doi:10.1016/B978-0-444-53831-4.00005-7

Narayanan, V., Anirudhan, S., and Grottoli, A. G. (2007). Oxygen and Carbon Isotope Analysis of the Miocene Limestone of Kerala and Its Implications to Palaeoclimate and Its Depositional Setting. *Curr. Sci.* 93, 1155–1159.

Odling, N. E., Gillespie, P., Bourgine, B., Castaing, C., Chilés, J. P., Christensen, N. P., et al. (1999). Variations in fracture system geometry and their implications for fluid flow in fractures hydrocarbon reservoirs. *Pet. Geosci.* 5, 373–384. doi:10.1144/petgeo.5.4.373

O'Neil, J. R., Clayton, R. N., and Mayeda, T. K. (1969). Oxygen Isotope Fractionation in Divalent Metal Carbonates. *J. Chem. Phys.* 51, 5547–5558. doi:10.1063/1.1671982

Pellaton, C. (1982). *Explanatory Notes to the Geologic Map of the UmmLajj Quadrangle, Sheet 25B,*. Kingdom of Saudi Arabia: Ministry of Petroleum and Mineral Resources Deputy Ministry for Mineral Resources.

Phillips, D. C. (1972). The Fracture Energy of Carbon-Fibre Reinforced Glass. *J. Mat. Sci.* 7, 1175–1191. doi:10.1007/BF00550201

Quandt, D., Micheuz, P., Kurz, W., Kluge, T., Boch, R., Hippler, D., et al. (2019). Geochemistry of Vein Calcites Hosted in the Troodos Pillow Lavas and Their Implications for the Timing and Physicochemical Environment of Fracturing, Fluid Circulation, and Vein Mineral Growth. *Geochem. Geophys. Geosyst.* 20, 5913–5938. doi:10.1029/2019GC008369

Reuning, L., Schoenherr, J., Heimann, A., Urai, J. L., Littke, R., Kukla, P. A., et al. (2009). Constraints on the Diagenesis, Stratigraphy and Internal Dynamics of the Surface-Piercing Salt Domes in the Ghaba Salt Basin (Oman): A Comparison to the Ara Group in the South Oman Salt Basin. *GeoArabia* 14, 83–120. doi:10.2113/geoarabia140383

Sharp, Z. D., Masson, H., and Lucchini, R. (2005). Stable Isotope Geochemistry and Formation Mechanisms of Quartz Veins; Extreme Paleoaltitudes of the Central Alps in the Neogene. *Am. J. Sci.* 305, 187–219. doi:10.2475/ajs.305.3.187

Shen, H., Wang, H., Wen, L., Ma, H., Li, Y., and Zhang, B. (2016). Natural Gas Exploration Prospect in the Upper Paleozoic Strata, NW Sichuan Basin. *Nat. Gas. Ind. B* 3, 526–536. doi:10.1016/j.ngib.2017.05.002

Sibley, D. F., and Gregg, J. M. (1987). Classification of Dolomite Rock Textures. *J. Sediment. Pet.* 57, 967–975. doi:10.1306/212f8cba-2b24-11d7-8648000102c1865d

Sibson, R. H. (1977). Fault Rocks and Fault Mechanisms. *J. Geol. Soc. Lond.* 133, 191–213. doi:10.1144/gsjgs.133.3.0191

Smith, D. A. (1980). Sealing and Nonsealing Faults in Louisiana Gulf Coast Salt Basin. *Am. Assoc. Pet. Geol. Bull.* 64, 145–172. doi:10.1306/2f918946-16ce-11d7-8645000102c1865d

Stanienda-Pilecki, K. J. (2018). Magnesium Calcite in Muschelkalk Limestones of the Polish Part of the Germanic Basin. *Carbonates Evaporites* 33, 801–821. doi:10.1007/s13146-018-0437-y

Stacey, J., Hollis, C., Corlett, H., and Koeshidayatullah, A. (2021a). Burial dolomitization driven by modified seawater and basal aquifer-sourced brines: Insights from the Middle and Upper Devonian of the Western Canadian Sedimentary Basin. *Basin Res.* 33 (1), 648–680.

Stacey, J., Corlett, H., Holland, G., Koeshidayatullah, A., Cao, C., Swart, P., et al. (2021b). Regional fault-controlled shallow dolomitization of the Middle Cambrian Cathedral Formation by hydrothermal fluids fluxed through a basal clastic aquifer. *GSA Bulletin* 133 (11-12), 2355–2377.

Stewart, D. R. M., Pearson, P. N., Ditchfield, P. W., and Singano, J. M. (2004). Miocene Tropical Indian Ocean Temperatures: Evidence from Three Exceptionally Preserved Foraminiferal Assemblages from Tanzania. *J. Afr. Earth Sci.* 40, 173–189. doi:10.1016/j.jafrearsci.2004.09.001

Suchy, V., Heijlen, W., Sykorova, I., Muchez, P., Dobes, P., Hladikova, J., et al. (2000). Geochemical Study of Calcite Veins in the Silurian and Devonian of the Barrandian Basin (Czech Republic): Evidence for Widespread Post-Variscan Fluid Flow in the Central Part of the Bohemian Massif. *Sediment. Geol.* 131, 201–219. doi:10.1016/S0037-0738(99)00136-0

Swart, P. K. (2015). The Geochemistry of Carbonate Diagenesis: The Past, Present and Future. *Sedimentology* 62, 1233–1304. doi:10.1111/sed.12205

Tsang, C.-F., Stephansson, O., and Hudson, J. A. (2000). A Discussion of Thermo–Hydro–Mechanical (THM) Processes Associated with Nuclear Waste Repositories. *Int. J. Rock Mech. Min. Sci.* 37, 397–402. doi:10.1016/s1365-1609(99)00114-8

Tsang, C. F. (2005). Is Current Hydrogeologic Research Addressing Long-Term Predictions? *Ground Water* 43, 296–300. doi:10.1111/j.1745-6584.2005.0023.x

Tubbs, R. E., Fouda, H. G. A., Afifi, A. M., Raterman, N. S., Hughes, G. W., and Fadolalkarem, Y. K. (2014). Midyan Peninsula, Northern Red Sea, Saudi Arabia: Seismic Imaging and Regional Interpretation. *GeoArabia* 19, 165–184. doi:10.2113/geoarabia1903165

Vandeginste, V., and John, C. M. (2012). Influence of Climate and Dolomite Composition on Dedolomitization: Insights from a Multi-Proxy Study in the Central Oman Mountains. *J. Sediment. Res.* 82, 177–195. doi:10.2110/jsr.2012.19

Vandeginste, V., Stehle, M. C., Jourdan, A. L., Bradbury, H. J., Manning, C., and Cosgrove, J. W. (2017). Diagenesis in Salt Dome Roof Strata: Barite - Calcite Assemblage in Jebel Madar, Oman. *Mar. Pet. Geol.* 86, 408–425. doi:10.1016/j.marpetgeo.2017.06.008

Vérard, C., and Veizer, J. (2019). On Plate Tectonics and Ocean Temperatures. *Geology* 47, 881–885. doi:10.1130/G46376.1

Vita-Finzi, C. (2001). Neotectonics at the Arabian Plate Margins. *J. Struct. Geol.* 23, 521–530. doi:10.1016/S0191-8141(00)00117-6

Vrolijk, P., and Sheppard, S. M. F. (1991). Syntectonic Carbonate Veins from the Barbados Accretionary Prism (ODP Leg 110): Record of Palaeohydrology. *Sedimentology* 38, 671–690. doi:10.1111/j.1365-3091.1991.tb01014.x

Wagner, T., Boyce, A. J., and Erzinger, J. (2010). Fluid-Rock Interaction during Formation of Metamorphic Quartz Veins: A REE and Stable Isotope Study from the Rhenish Massif, Germany. *Am. J. Sci.* 310, 645–682. doi:10.2475/07.2010.04

Warren, J. (2000). Dolomite: Occurrence, Evolution and Economically Important Associations. *Earth Sci. Rev.*

Weyhenmeyer, C. E., Burns, S. J., Waber, H. N., Aeschbach-Hertig, W., Kipfer, R., Loosli, H. H., et al. (1979). Cool Glacial Temperatures and Changes in Moisture Source Recorded in Oman Groundwaters. *Science* 287, 842–845. doi:10.1126/science.287.5454.842

Woodcock, N. H., Omma, J. E., and Dickson, J. A. D. (2006). Chaotic Breccia along the Dent Fault, NW England: Implosion or Collapse of a Fault Void? *J. Geol. Soc. Lond.* 163, 431–446. doi:10.1144/0016-764905-067

Wu, G., Xie, E., Zhang, Y., Qing, H., Luo, X., and Sun, C. (2019). Structural Diagenesis in Carbonate Rocks as Identified in Fault Damage Zones in the Northern Tarim Basin, NW China. *Minerals* 9, 360. doi:10.3390/min9060360

Zachos, J. C., Stott, L. D., and Lohmann, K. C. (1994). Evolution of Early Cenozoic Marine Temperatures. *Paleoceanography* 9, 353–387. doi:10.1029/93PA03266

Zhu, D., Liu, Q., Zhang, J., Ding, Q., He, Z., and Zhang, X. (2019). Types of Fluid Alteration and Developing Mechanism of Deep Marine Carbonate Reservoirs. *Geofluids* 2019, 1–18. doi:10.1155/2019/3630915

Zierenberg, R. A., and Shanks, W. C. (1983). Mineralogy and Geochemistry of Epigenetic Features in Metalliferous Sediment, Atlantis II Deep, Red Sea. *Econ. Geol.* 78, 57–72. doi:10.2113/gsecongeo.78.1.57